Interference effects in a double quantum dot system with inter-dot Coulomb correlations

2007 J. Phys.: Condens. Matter 19 176202

(http://iopscience.iop.org/0953-8984/19/17/176202)

IOP PUBLISHING JOURNAL OF PHYSICS: CONDENSED MATTER

J. Phys.: Condens. Matter **19** (2007) 176202 (12pp) doi:10.1088/0953-8984/19/17/176202

Interference effects in a double quantum dot system with inter-dot Coulomb correlations

D Sztenkiel and R Świrkowicz

Faculty of Physics, Warsaw University of Technology, ulica Koszykowa 75, 00-662, Warsaw, Poland

E-mail: DSZ@poczta.fm

Received 10 January 2007, in final form 20 February 2007
Published 28 March 2007
Online at stacks.iop.org/JPhysCM/19/176202

Abstract

Electron transport through a double quantum dot system is studied with the use of the Green function formalism based on the equation of motion method, and an interplay between interference and Coulomb blockade effects due to inter-dot correlations is discussed. A double structure with two Fano resonances (or antiresonances) is found in the conductance spectrum. Fano features are weakly influenced by the presence of Coulomb interaction but the conductance is strongly suppressed in the energy region with the Fermi level in the leads close to the aligned levels of both dots. This Coulomb blockade effect takes place when the coupling between the dots is of repulsive character. On the other hand, the conductance of an artificial molecule with attractive inter-dot coupling is only slightly modified in this energy region. As a sign of the coupling can be easily changed in a presence of an external magnetic field by changes of the magnetic flux there is the possibility to control variations of the conductance, which may be important from the application point of view.

1. Introduction

Recently, due to advances in nanotechnology, the Fano resonance in electron transport through nanoscopic devices has attracted considerable attention [1–6]. The effect results from quantum interferences between resonant and non-resonant processes and can be observed in systems of a special geometry with at least two scattering channels. Fano resonance manifests itself in conductance spectra of such systems as an asymmetric line of a particular shape. Fano-like features as well as interference effects were investigated in an Aharonov–Bohm (A–B) interferometer with a quantum dot (QD) embedded in a one arm of the interferometer, in double quantum dot (DQD) structures, or in other nanoscale devices in which quantum coherence phenomena play an important role [1–6]. The coherence of quantum mechanical states has recently gained a broad interest as it is important for quantum computation [7]. Oscillations of the current in the presence of magnetic flux in A–B interferometers containing one or two QDs are evidences for coherent transport, and such systems enable investigations of the phase

coherence. Fano resonance also appears to be a very good probe of the phase coherence in QDs [8]. Moreover, in such systems the key parameters which strongly influence the Fano effect can be easily tuned, which offers new possibilities which are not accessible in a conventional set-up. Johnson *et al* studied a tunable interferometer consisting of a QD coupled in a tunnel way to a one-dimensional channel and observed a series of Fano resonances [1]. Similarly, Kobayashi *et al* investigated the tunable Fano effect in a QD embedded in an A–B ring [2], whereas Zacharia *et al* analysed in detail interference effects in a tunable single-electron transistor with weak coupling to the leads [3]. DQD systems are especially interesting as each of the QDs can be manipulated separately, which increases the number of key parameters in comparison to single-dot interferometers [6]. In particular, the inter-dot coupling, which influences the Fano line shape considerably, can be tuned with the use of gate voltages [9]. The observation of the Kondo effect in strongly coupled DQD systems was interpreted as evidence for spin entanglement between the excess electrons on each dot [10]. The lateral transport through strongly vertically coupled QDs reveals both Kondo and Fano effects [11]. The observation of both effects in one device offers the possibility to study interference and many-body effects in the same system. The entanglement phenomenon versus the Kondo effect in DQD systems of various topology have been studied theoretically very recently [12]. The problem is of current interest as nanostructures consisting of coupled QDs seem to be very good candidates for solid-state arrays of qubits [7]. Fano features in the conductance spectrum due to interference processes between possible pathways for electrons tunnelling through two exchange split states in diatomic molecule can be used to detect singlet–triplet splitting in such molecules, as has been recently proposed by Fransson and Balatsky [13].

The Fano effect in DQD systems of various topology has been a subject of intensive studies during the last few years, and various theoretical approaches have been proposed [8, 13–34]. Kubala and Konig reported a level attraction in an A–B interferometer with two QDs [14], whereas Ladron de Guevara *et al* [15] have investigated electronic transport across DQD structures and discussed modifications of the Fano resonance during a gradual transition from a series to a parallel configuration of two dots coupled via tunnelling processes. The presence of two different pathways accessible for the electron transport leads to conductance spectra composed of Breit–Wigner and Fano-like resonance peaks which correspond to bonding and antibonding molecular states, respectively. A progressive line narrowing of the Fano peak can be observed as the system transits from the series to the parallel arrangement. Applying a magnetic field to a double dot structure in the parallel configuration allows one to interchange the roles of the bonding and antibonding states in the transmission spectrum by changing the magnetic flux by 2π and this swap effect might be of potential application in quantum computation [18, 35]. Orellana *et al* considered electron transport through a DQD region asymmetrically coupled to the leads [20]. It was shown that the observed Fano and Dicke effects can be controlled by the magnetic flux. Resonant tunnelling and Fano resonance in QDs in a presence of electron–phonon interaction has been studied very recently by Ueda and Eto, who have found a strong influence of acoustic phonons on the Fano line shape [23]. No Coulomb interaction between electrons was taken into account in all these approaches [8, 14–23]. Coupled parallel QD systems with on-site Coulomb correlations included within the framework of the Hartree–Fock approximation have been studied quite recently, and an additional Fano resonance resulting from interferences between Coulomb blockade peaks has been found [24]. An influence of quantum interferences on spin-polarized transport across a DQD region attached to magnetic electrodes has been also studied [25, 26]. The interplay between interference and interaction effects due to on-site Coulomb interactions has also been investigated in a more rigorous approach, and the coexistence of Fano and Kondo resonance peaks has been discussed [27–33].

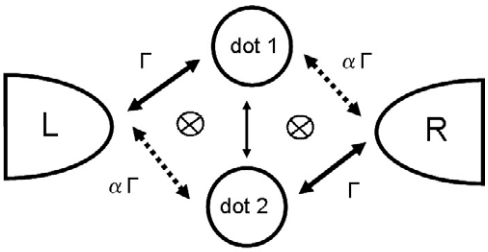

Figure 1. Schematic diagram of double quantum dots coupled to left (L) and right (R) leads.

Theoretical studies of the Fano effect in coupled QDs have mainly been performed for non-interacting systems or correlated ones with on-site Coulomb interaction taken into account, whereas the effects of inter-dot correlations were often neglected. Some investigations concerning two QDs in a parallel geometry with intra- and inter-dot interaction included in the Kondo regime have been undertaken, but no direct coupling between the dots was taken into account [36–38]. Generally, inter-dot Coulomb correlations are weaker than the on-site ones, and moreover, the correlation strength can be controlled in the experimental set-up. Their role may be important in studies of the Fano effect as the coupling strength between dots can be comparable to the Coulomb interaction.

In the present work, a theoretical study of the Fano effect in a DQD system with inter-dot Coulomb interaction taken into account is addressed. A special geometry which allows a transition from the series to the parallel configuration of two dots coupled via tunnelling processes is assumed (figure 1). Calculations are performed with use of the Green function (GF) formalism based on the equation of motion (EOM) method. A standard Hartree–Fock procedure is used, so the approach is appropriate for temperatures higher than the Kondo temperature. Limits of intermediate and weak coupling between the dots are discussed, and Fano resonance or antiresonance is found in these two regimes, respectively. Due to inter-dot Coulomb interactions between electrons, described by the parameter U, additional Fano features are obtained in conductance spectra for energies corresponding to molecular states shifted by U. Calculations performed in the intermediate regime show that the Fano resonance is weakly influenced by inter-dot Coulomb interaction, and only a slight lowering of the peak intensity can be observed for $U \to \infty$. However, the behaviour of the linear conductance apart from the resonance strongly depends on the sign of the inter-dot coupling t. The conductance of an artificial molecule (with the attractive coupling between the dots $t < 0$) remains practically unchanged in the energy region where the Fermi level in the leads E_{F} is close to the aligned levels of both dots E_0, whereas in the case $t > 0$ a strong suppression of the conductance is obtained in this energy region due to correlation effects. As the sign of t can be easily changed in the presence of a magnetic flux there is the possibility to control variations of the conductance in correlated systems. Significant suppression of the conductance in the vicinity of $E_{\mathrm{F}} \approx E_0$ when the magnetic flux changes by 2π would indicate that in the system under consideration correlation effects play an important role.

2. Model

The system under consideration, which consists of two QDs coupled via tunnelling processes and attached to external leads, is schematically presented in figure 1. It is described by the Hamiltonian

$$H = H_{\mathrm{L}} + H_{\mathrm{R}} + H_{\mathrm{DQD}} + H_{\mathrm{T}}. \tag{1}$$

The term H_β with $\beta = \mathrm{L}, \mathrm{R}$ describes the left ($\beta = \mathrm{L}$) and the right ($\beta = \mathrm{R}$) electrodes in the

non-interacting approximation and is taken in the form $H_\beta = \sum_k \varepsilon_{k\beta} a^\dagger_{k\beta} a_{k\beta}$. $a^\dagger_{k\beta}$ ($a_{k\beta}$) denotes here the creation (annihilation) operator of an electron with the wavenumber k in lead β, and $\varepsilon_{k\beta}$ is the corresponding single-particle energy.

H_{DQD} describes the two-dot region and is equal to

$$H_{\mathrm{DQD}} = \sum_{i=1,2} E_i d^\dagger_i d_i + t(d^\dagger_1 d_2 + d^\dagger_2 d_1) + U d^\dagger_1 d_1 d^\dagger_2 d_2. \tag{2}$$

We assume that only one energy level E_i in dot i ($i = 1, 2$) is active in the transport. In the above expression $d^\dagger_i$ (d_i) denotes the creation (annihilation) operator of an electron in dot i, and t is the strength of tunnelling coupling between dots. Inter-dot Coulomb interaction between electrons is taken in the Hubbard form and is described by the last term in Hamiltonian (2). Empty or singly occupied states are considered and the appropriate terms corresponding to on-site Coulomb interactions are omitted in equation (2).

Tunnelling processes between the DQD region and external electrodes are described by H_{T}, which represents the last term in the full Hamiltonian of the system (equation (1)) and is taken in the form

$$H_{\mathrm{T}} = \sum_{\substack{k,i=1,2 \\ \beta=\mathrm{L,R}}} (T_{k\beta i} a^\dagger_{k\beta} d_i + T^*_{k\beta i} d^\dagger_i a_{k\beta}) \tag{3}$$

where $T_{k\beta i}$ are elements of the matrix describing tunnelling processes between the electrode β ($=$ L, R) and dot i. In a general case an external magnetic field can be applied to the system; then a phase shift due to the magnetic flux is included in these coefficients [18]. Elements $T_{k\beta i}$ are directly related to tunnelling rates $\Gamma^\beta_{ii'}$ defined as follows: $\Gamma^\beta_{ii'}(\varepsilon) = 2\pi \sum_k T_{k\beta i} T^*_{k\beta i'} \delta(\varepsilon - \varepsilon_{k\beta})$, which are treated here as independent of energy. Couplings to electrodes are then expressed by the matrices: $\hat{\Gamma}^{\mathrm{L}} = \Gamma \begin{pmatrix} 1 & \sqrt{\alpha} \mathrm{e}^{\mathrm{i}\phi/2} \\ \sqrt{\alpha} \mathrm{e}^{-\mathrm{i}\phi/2} & \alpha \end{pmatrix}$ and $\hat{\Gamma}^{\mathrm{R}} = \Gamma \begin{pmatrix} \alpha & \sqrt{\alpha} \mathrm{e}^{-\mathrm{i}\phi/2} \\ \sqrt{\alpha} \mathrm{e}^{\mathrm{i}\phi/2} & 1 \end{pmatrix}$. When α is changed from 0 to 1 a transition from a serial to a parallel configuration of two dots can be realized (figure 1). For $0 < \alpha \leqslant 1$ two paths are possible, which leads to interference effects, and non-diagonal matrix elements $\Gamma^\beta_{ii'}$ with $i \neq i'$ are different from zero. A phase shift due to the magnetic flux is included into non-diagonal terms and $\phi = 2\pi\Phi/\Phi_0$, where Φ and Φ_0 are the external flux through the system and the flux quantum, respectively.

The Green function formalism based on the equation of motion method is applied to study the electron transport. The current flowing through the system in the presence of a bias voltage is calculated according to a formula derived by Meir [39] (details of the calculations are given in the appendix):

$$I = i\frac{2e}{\hbar} \int \frac{\mathrm{d}\varepsilon}{2\pi} \frac{1}{2} \mathrm{Tr}\{(\hat{\Gamma}^{\mathrm{L}} - \hat{\Gamma}^{\mathrm{R}})\hat{G}^<(\varepsilon) + [\hat{\Gamma}^{\mathrm{L}} f_{\mathrm{L}}(\varepsilon) - \hat{\Gamma}^{\mathrm{R}} f_{\mathrm{R}}(\varepsilon)][\hat{G}^{\mathrm{r}}(\varepsilon) - \hat{G}^{\mathrm{a}}(\varepsilon)]\}. \tag{4}$$

f_β represents here the Fermi–Dirac distribution function and the matrix $\hat{G}^j$ with elements $G^j_{ii'} = \langle\langle d_i, d^\dagger_{i'} \rangle\rangle^j_\varepsilon$ denotes the Fourier transform of the retarded, advanced and lesser Green function for $j = r, a, <$, respectively. Retarded and advanced Green functions are calculated with use of the EOM method [40–42]. A standard Hartree–Fock procedure is employed to decouple higher-order functions which contain $a^\dagger_{k\beta}$, $a_{k\beta}$ operators apart from d_i ones. However, no decoupling is introduced for functions of the type $\langle\langle d_{i'} d^\dagger_{-i'} d_{-i'}, d^\dagger_i \rangle\rangle$, and they are calculated according to appropriate second-order equations. Solutions of the set of equations of motion can be written in the following form which corresponds to the Dyson equation (for details see the appendix):

$$\hat{G}(\varepsilon) = [\hat{I} - \hat{g}(\varepsilon)\hat{\Sigma}(\varepsilon)]^{-1} \hat{g}(\varepsilon). \tag{5}$$

$\hat{g}(\varepsilon)$ with elements $g_{ii'}(\varepsilon) = \delta_{ii'}(\varepsilon - E_i)^{-1}$ represents here the Green function of the dots in the absence of any coupling or interaction. All correlation and tunnel effects are included into the self-energy $\hat{\Sigma}$ which is given by the expression

$$\hat{\Sigma}(\varepsilon) = \hat{g}^{-1} - [\hat{g}_U^{-1} - \hat{T} - U\hat{\tilde{n}}]^{-1}(\hat{g}_U^{-1} - \hat{T})(\hat{g}^{-1} - \hat{T}) + \hat{\Sigma}_0. \tag{6}$$

$\hat{\Sigma}_0$ with elements $\Sigma_{0ii'} = \sum_{k\beta=\mathrm{L,R}} \frac{T_{k\beta i} T^*_{k\beta i'}}{\varepsilon - \varepsilon_{k\beta}}$ denotes here the self-energy of the non-interacting system, $g_{U_{ii'}} = \delta_{ii'}(\varepsilon - E_i - U)^{-1}$, $T_{ii'} = \delta_{i-i'}t$ and $\tilde{n}_{ii} = -\langle d^\dagger_{-i} d_{-i}\rangle$, $\tilde{n}_{i-i} = \langle d^\dagger_{-i} d_i\rangle$. To calculate the mean value $\langle d_i^\dagger d_{i'}\rangle$ defined as follows: $\langle d_i^\dagger d_{i'}\rangle = -\mathrm{i}\int \frac{\mathrm{d}\varepsilon}{2\pi} G^<_{i'i}$, the lesser Green function $G^<_{i'i}$ should be known. In the present approach the function is determined according to the Keldysh equation $\hat{G}^< = \hat{G}^\mathrm{r}\hat{\Sigma}^<\hat{G}^\mathrm{a}$ with the Ng ansatz [43] used for $\hat{\Sigma}^<$, namely $\hat{\Sigma}^< = \hat{\Sigma}_0^<\hat{\Gamma}^{-1}\hat{\Gamma}^{ef}$ where $\Sigma_0^< = \mathrm{i}(\hat{\Gamma}^\mathrm{L} f_\mathrm{L} + \hat{\Gamma}^\mathrm{R} f_\mathrm{R})$, $\hat{\Gamma} = \hat{\Gamma}^\mathrm{L} + \hat{\Gamma}^\mathrm{R} = \mathrm{i}(\hat{\Sigma}_0^\mathrm{r} - \hat{\Sigma}_0^\mathrm{a})$ and $\hat{\Gamma}^{ef} = \mathrm{i}(\hat{\Sigma}^\mathrm{r} - \hat{\Sigma}^\mathrm{a})$. The advanced Green function $\hat{G}^\mathrm{a}$ and the retarded one $\hat{G}^\mathrm{r} = (\hat{G}^\mathrm{a})^\dagger$ are calculated from the Dyson equation (5). The knowledge of $\hat{G}^<$ allows one to calculate electric current according to equation (4). In the following we limit the discussion to the linear conductance G given by

$$G = \frac{2e^2}{h}\int \frac{\mathrm{d}\varepsilon}{2\pi}\frac{1}{2}\mathrm{Tr}[\hat{\Gamma}^\mathrm{L}\hat{G}^\mathrm{r}\hat{\tilde{\Gamma}}^\mathrm{R}\hat{G}^\mathrm{a} + \hat{\Gamma}^\mathrm{R}\hat{G}^\mathrm{r}\hat{\tilde{\Gamma}}^\mathrm{L}G^\mathrm{a}]\left(-\frac{\partial f}{\partial \varepsilon}\right) \tag{7}$$

with $\hat{\tilde{\Gamma}}^\beta = \hat{\Gamma}^\beta\hat{\Gamma}^{-1}\hat{\Gamma}^{ef}$. The above expression can be easily obtained from equation (4) when the relations $\hat{G}^< = \hat{G}^\mathrm{r}\hat{\Sigma}_0^<\hat{\Gamma}^{-1}\hat{\Gamma}^{ef}\hat{G}^\mathrm{a}$ and $\hat{G}^\mathrm{r} - \hat{G}^\mathrm{a} = \hat{G}^\mathrm{r}(\hat{\Sigma}^\mathrm{r} - \hat{\Sigma}^\mathrm{a})\hat{G}^\mathrm{a} = -\mathrm{i}\hat{G}^\mathrm{r}\hat{\Gamma}^{ef}\hat{G}^\mathrm{a} = -\mathrm{i}\hat{G}^\mathrm{r}\hat{\Gamma}\hat{\Gamma}^{-1}\hat{\Gamma}^{ef}\hat{G}^\mathrm{a}$ are taken into account and the Fermi–Dirac functions are expanded in series with respect to the applied bias voltage: $f_\mathrm{L}(\varepsilon) - f_\mathrm{R}(\varepsilon) \approx -\frac{\partial f}{\partial \varepsilon}$ eV. Note that for the non-interacting system $\hat{\Gamma}^{ef} = \hat{\Gamma}$, and equation (7) reduces to the one used in [15].

3. Results and discussion

The interplay between correlation and interference effects is studied in two regimes of inter-dot tunnelling coupling, namely in the intermediate one with rate t being of the same order as the coupling of the DQD region with external electrodes described by Γ, and in a weak-coupling regime with $t \ll \Gamma$. The symmetric DQD system with energy levels of both dots aligned and equal to $E_1 = E_2 = E_0 = 0$ is discussed here. All parameters are measured in relative units and Γ describing the coupling of the DQD region with one of the leads is taken as the energy unit.

3.1. Intermediate-coupling regime

Consider first the case when the inter-dot tunnelling rate is of the same order as the coupling to external electrodes. The linear conductance G calculated as a function of the Fermi energy in the leads E_F for $t = \pm\Gamma$ and several values of parameter α is displayed in figure 2. To illustrate the influence of inter-dot Coulomb interaction curves obtained for the uncorrelated system ($U = 0$) and for the correlated one with $U = 5\Gamma$ are depicted (dotted and solid lines, respectively). Results presented for an artificial molecule with $t = -\Gamma$ and no interactions taken into account are well known from other approaches [15, 16]. Two molecular states, the bonding and antibonding ones with energies $E_0 + t$ and $E_0 - t$, are active in the transport, giving two peaks in the conductance for $\alpha = 0$ (inset in figure 2, dotted line). Interference effects present for $\alpha \neq 0$ due to different paths available in the system lead to Fano-like resonance shown by the antibonding peak (figures 2(a) and (b), dotted lines). In the case $t = \Gamma$ and

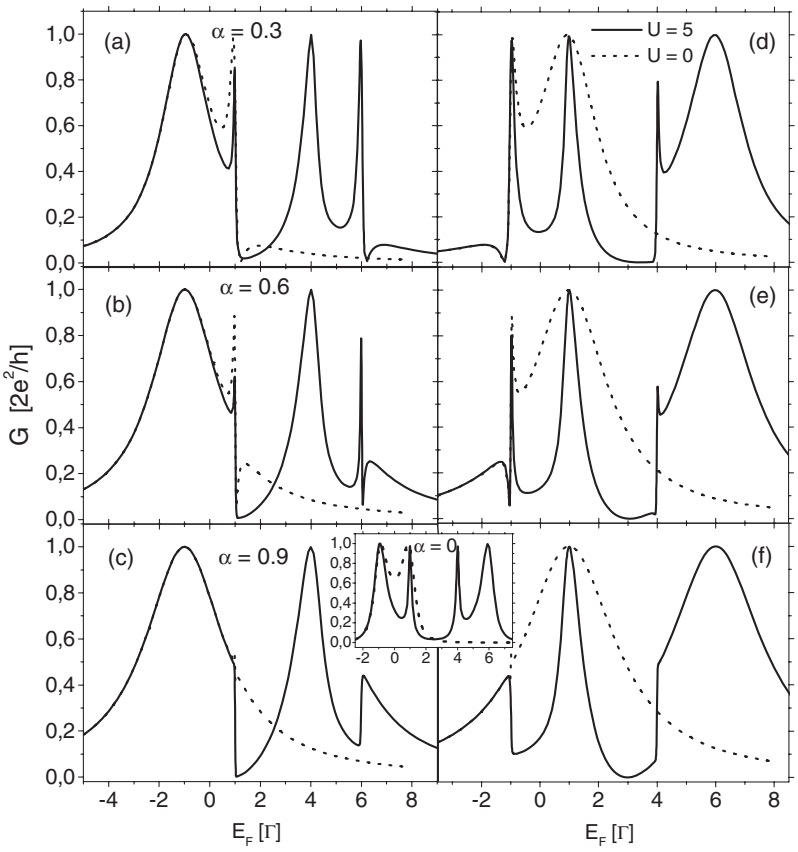

Figure 2. The linear conductance as a function of the Fermi energy E_F of uncorrelated ($U = 0$, dotted lines) and correlated ($U = 5\Gamma$, solid lines) systems for $kT = 0.01\Gamma$ and different values of α, (left panel: $t = -\Gamma$, and right panel: $t = \Gamma$).

$U = 0$, the lower energy corresponds to the state $E_0 - t$, and now this bonding peak develops into the Fano one when interference effects become important.

Let us now discuss modifications of the conductance G resulting from inter-dot Coulomb interactions. A typical conductance curve calculated for two dots in series with correlation effects included shows four peaks, the bonding and antibonding ones as well as the appropriate peaks shifted by U which result from the Coulomb repulsion (inset in figure 2, solid line). The widths of the peaks are different but their intensities are almost equal. Interferences present in the system for $\alpha \neq 0$ and $t = -\Gamma$ lead to a considerable broadening of the bonding peak at $E_0 + t$ as well as the one corresponding to energy $E_0 + t + U$, whereas the antibonding peaks centred at $E_0 - t$ and $E_0 - t + U$ become narrower and show a Fano-like behaviour (figures 2(a) and (b), solid lines). The intensities of both Fano resonances decrease as α increases, and for high values of α only the wide peaks are visible in the conductance spectrum. The bonding peak centred for an artificial molecule at energy $E_0 + t$ is very similar to the Breit–Wigner one observed in the non-interacting system. In the case when $t = \Gamma$, the Fano-like behaviour is shown by bonding peaks centred at $E_0 - t$ and $E_0 - t + U$, and their shapes correspond well to Fano resonance in a system with no correlation effects included. Similarly, the wide peak which appears at energy $E_0 + t + U$ resembles the Breit–Wigner resonance in the non-

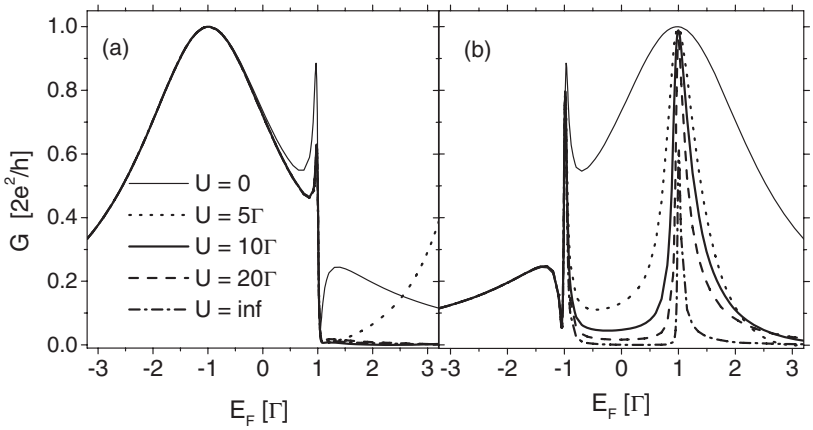

Figure 3. Conductance for $t = -\Gamma$ (a), $t = \Gamma$ (b) and indicated values of $U, \alpha = 0.6$ and $kT = 0.01\Gamma$.

interacting system. The intensities and widths of the peaks are almost equal in both cases, though they are shifted by U. However, the antibonding state with energy $E_0 + t$ leads to a relatively narrow peak, and in consequence a considerable suppression of the conductance in its vicinity is obtained (figure 2 right panel, solid lines).

The behaviour of bonding and antibonding states in correlated systems with interference effects taken into account is well illustrated in figure 3, where conductance curves are depicted for several values of U as well as for $t = -\Gamma$ and $t = \Gamma$. The range of energies presented in the figure is limited to a vicinity of $E_F \approx E_0 = 0$, and the situation with the energy level of both dots close to the Fermi level of the leads is considered. The figure illustrates very well the interplay between Coulomb blockade and interference effects. As could be expected, the bonding states, namely the wide resonance for $t = -\Gamma$ or the Fano peak for $t = \Gamma$, are practically not modified by Coulomb repulsion. It is also interesting that the Fano resonance related to the antibonding state with $t = -\Gamma$ is not essentially influenced by Coulomb blockade effects (figure 3(a)). However, the conductance is suppressed in the vicinity of the peak. In particular, the dip that is well visible in the spectrum of a non-interacting system directly after the peak is now considerably influenced and the conductance is strongly suppressed. So, in this energy region destructive interference effects are enhanced by Coulomb repulsion. Typical Coulomb blockade effects take place for $t = \Gamma$, where the antibonding state is considerably influenced by the presence of U (figure 3(b)). With increase of U the peak of Breit–Wigner type centred at $E_0 + t$ starts to narrow, and the conductance is considerably suppressed. In strongly correlated systems with $U \to \infty$ the conductance is close to zero in a valley between this peak and the Fano one associated with the bonding state. Note that the appropriate wide peak which resembles the Breit–Wigner resonance appears at $E_0 + t + U$ when the energy due to the gate voltage is sufficient to overcome the Coulomb repulsion (figures 2(d) and (e)).

Evolution of the conductance spectrum in the correlated system with $U = 5\Gamma$ under the magnetic field applied to the structure is presented in figure 4. For $\phi = 0$ and $\alpha = 0.3$, a curve showing two Fano-like resonances related to the bonding states is obtained (figure 2(d), $t = \Gamma$). As ϕ increases, the Fano peaks become wider, whereas the peak centred at $E_0 + t + U$, and resembling the Breit–Wigner resonance, starts to narrow. For $\phi = \pi$ no features typical of interference effects can be seen in the spectrum. The shape of the conductance curve resembles very closely the one obtained for $\alpha = 0$ (see the inset in figure 2), though both spectra are not identical. When ϕ increases further, Fano resonance peaks develop, but now they are related

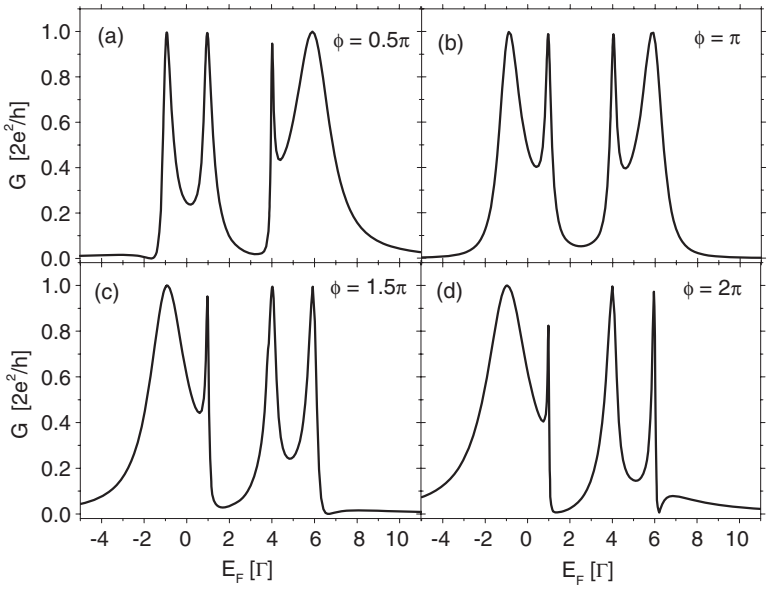

Figure 4. Conductance as a function of the Fermi energy E_F for $t = \Gamma$ and different values of magnetic flux, $kT = 0.01\Gamma$, $U = 5\Gamma$ and $\alpha = 0.3$.

to antibonding states. Therefore, a change of magnetic flux by 2π corresponds to a transition from $t = \Gamma$ to $-\Gamma$. Such changes lead to considerable modifications of the spectrum in the energy region with $E_F \approx E_0$ due to Coulomb blockade effects.

3.2. Weak-coupling regime

Consider now a weak-coupling regime with inter-dot tunnelling rate t much smaller than the coupling to external electrodes. The results calculated in this case look different from the ones obtained in the limit of intermediate coupling ($t = \pm\Gamma$), which is well illustrated in figure 5, where conductance spectra are presented for several values of α. Consider first a non-interacting system with two dots in series and inter-dot rate $t = -0.1\Gamma$. The conductance shows the low-intensity peak centred at E_0 as bonding and antibonding states cannot be resolved due to the small inter-dot tunnelling rate (figure 5(a), dotted line). Strong modifications of G are obtained for $\alpha \neq 0$. As an additional path is accessible for electron transport the conductance is considerably enhanced and a high-resonance peak can be seen. The peak is followed by a relatively wide dip which appears in a close vicinity of E_0 due to destructive interference effects. As α increases, the peak intensity also increases approaching $2e^2/h$, whereas the dip becomes less pronounced and narrower. For $\alpha = 0.9$, one broad and high peak is obtained and the dip is hardly visible. The results presented here for a non-interacting system can be easily explained. As was shown in [15, 16], the Fano factor q which determines the line shape is simply proportional to the inter-dot coupling t in such a case. For a small t/Γ ratio the appropriate Fano factor is small, and it corresponds to antiresonance in the spectrum.

The influence of the correlation effects on the calculated conductance curves is also presented in figure 5 for $t = -0.1\Gamma$ and $U = 5\Gamma$. As could be expected, the Coulomb interactions modify the conductance of two dots in series, leading to the appearance of an additional peak centred at $E_0 + U$. For $\alpha = 0$, the intensities of both peaks are small, though a bit higher than in the non-interacting case. When interference effects play an important role

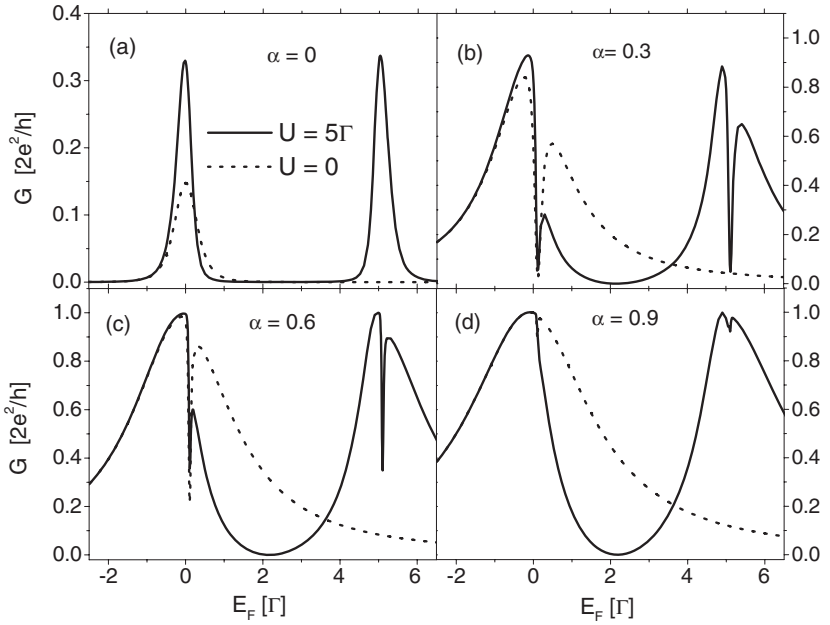

Figure 5. Conductance of uncorrelated ($U = 0$, dotted lines) and correlated ($U = 5\Gamma$, solid lines) systems for indicated values of α and $t = -0.1\Gamma$, $kT = 0.01\Gamma$.

($\alpha \neq 0$), two resonance peaks centred near E_0 and $E_0 + U$ can be seen, which are followed by well pronounced dips. As α increases, the behaviour of both peaks and dips is similar to that in the non-interacting case. The results obtained for $t = 0.1\Gamma$ are very similar, but the positions of peaks and dips are interchanged.

The influence of the temperature on the calculated conductance is presented in figure 6 for $U = 5\Gamma$ and $t = 0.1\Gamma$. At low temperatures, due to destructive interference effects the conductance is suppressed considerably for E_F close to E_0 or $E_0 + U$, and the dips are very well pronounced. As kT increases, the role of interferences is less important because of thermal broadening, and the dips become shallow, but they are still visible for intermediate values of α. Note that for a relatively high temperature no dip appears in the conductance spectra in the vicinity of $E_0 + U$, though small dips are still present near E_0 for $\alpha = 0.3$ and 0.6 (figure 6(d)).

4. Summary and conclusions

Studies performed in this paper clearly show that correlation effects due to inter-dot Coulomb interaction lead to a double structure with two Fano-like resonances or antiresonances. In the intermediate regime with $t = \pm\Gamma$, constructive interferences lead to the Fano resonance which appears at energy $E_0 - t$. Due to inter-dot Coulomb interactions, an additional Fano peak can be observed at energy $E_0 - t + U$. The result is well consistent with the one obtained by Lu *et al*, who discussed the influence of on-site Coulomb interaction on the linear conductance in the presence of a magnetic flux [24]. Further calculations presented in this paper show that the Fano resonances are weakly influenced by the inter-dot correlations. However, one of the peaks of Breit–Wigner type, centred at $E_0 + t$, is strongly narrowed when t is positive, and due to Coulomb blockade the conductance is considerably suppressed in the valley between this peak and the appropriate Fano resonance. In strongly correlated systems, G is practically equal to

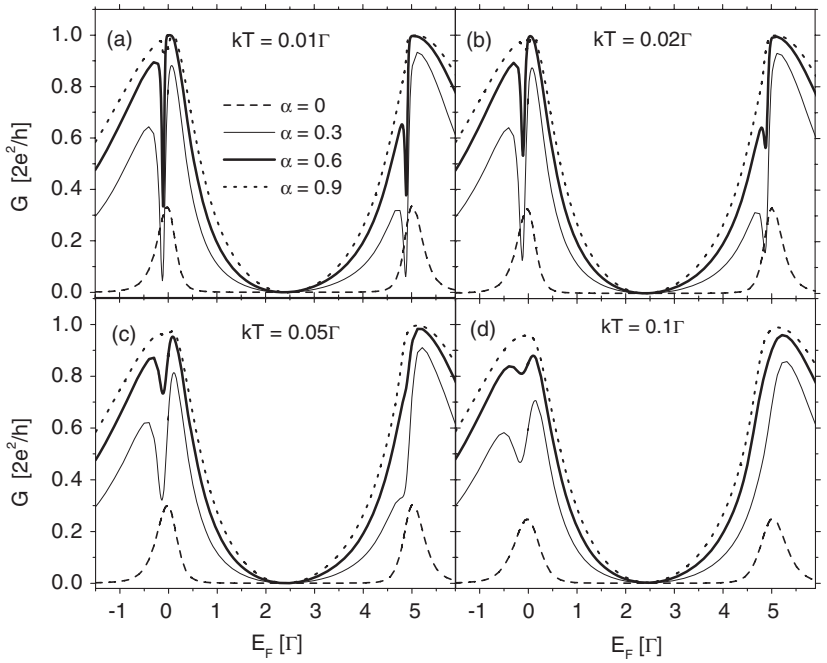

Figure 6. The linear conductance as a function of the Fermi energy E_{F} for indicated values of temperature and α. The relevant parameters are as follows: $t = 0.1\Gamma$, $U = 5\Gamma$.

zero in the energy region between the two peaks. In double-dot systems the inter-dot correlation parameter U is determined by the relation of the inter-dot capacitance C_{12} to the capacitances of individual dots C_1 and C_2, and it can be controlled in an experimental set-up. Therefore, the conductance of the system can also be controlled, and a regime where the conductance is close to zero may be achieved. When a magnetic field is applied to a DQD structure a change of the magnetic flux by 2π corresponds to a transition $t \to -t$ and leads to considerable variations of the conductance in the energy region $E_{\mathrm{F}} \approx E_0$. Therefore, in a double-dot system there is the possibility to control variations of the conductance in a wide range between zero and $2e^2/h$ by changes of magnetic flux by 2π, which may be important from an application point of view.

The results obtained in the weak-coupling regime look different. A well pronounced dip appears near energy E_0 as a result of destructive interferences. Since the additional path is accessible for electron transport when $\alpha \neq 0$, the conductance is strongly enhanced, but the resonance peak is associated with the dip. Inter-dot Coulomb correlations modify the conductance curves, leading to a double structure with two dips and appropriate resonance peaks. As in experimental set-ups in which two dots are coupled in an electrostatic way the inter-dot rate can be easily tuned, the conductance of the system can show a different behaviour depending on the parameters.

Appendix

The current flowing through the system from the lead β is given by the time derivative of the occupation number in the lead, namely

$$I_\beta = -e\left\langle \frac{\mathrm{d}N_\beta}{\mathrm{d}t} \right\rangle = -\mathrm{i}\frac{e}{\hbar}\langle H, N_\beta \rangle \tag{A.1}$$

with $N_\beta = \sum_k a^\dagger_{k\beta} a_{k\beta}$. Taking into account Hamiltonian (1) and introducing the lesser Green function defined as follows: $G^<_{ik\beta}(t,t') = \mathrm{i}\langle a^\dagger_{k\beta}(t') d_i(t)\rangle$, one can express the current in the form

$$I_\beta = \frac{2e}{\hbar}\,\mathrm{Re}\sum_{ki} T_{k\beta i} G^<_{ik\beta}(t,t). \tag{A.2}$$

When the Fourier transform of the $G^<$ is introduced and the Langreth theorem is applied: $G^<_{ik\beta}(\varepsilon) = \sum_{i'} T^*_{k\beta i'}[G^<_{ii'}(\varepsilon) g^{\mathrm{a}}_{k\beta}(\varepsilon) + G^{\mathrm{r}}_{ii'}(\varepsilon) g^<_{k\beta}(\varepsilon)]$, the current becomes equal to (details of calculations are given in [40])

$$I_\beta = \frac{2e}{\hbar}\,\mathrm{Re}\sum_{kii'}\int \frac{\mathrm{d}\varepsilon}{2\pi} T^*_{k\beta i'} T_{k\beta i}[G^<_{ii'}(\varepsilon) g^{\mathrm{a}}_{k\beta}(\varepsilon) + G^{\mathrm{r}}_{ii'}(\varepsilon) g^<_{k\beta}(\varepsilon)]. \tag{A.3}$$

In the above formula, $G^{\mathrm{r}}_{ii'}(\varepsilon) = \langle\langle d_{i'}, d^\dagger_i\rangle\rangle^{\mathrm{r}}_\varepsilon$ denotes the Fourier transform of the retarded GF and $g^{\mathrm{a}}_{k\beta}(\varepsilon) = (\varepsilon - \varepsilon_{k\beta} - \mathrm{i}\eta)^{-1}$ and $g^<_{k\beta}(\varepsilon) = 2\pi\mathrm{i} f_\beta(\varepsilon)\delta(\varepsilon - \varepsilon_{k\beta})$ are advanced and lesser functions corresponding to the electrode β with $f_\beta(\varepsilon)$ being the Fermi–Dirac distribution function. Taking into account the definition of elements of $\Gamma^\beta_{ii'}$, one can finally express the current in the form (see also [39])

$$I = \mathrm{i}\frac{2e}{\hbar}\int \frac{\mathrm{d}\varepsilon}{2\pi}\frac{1}{2}\,\mathrm{Tr}\{(\hat\Gamma^{\mathrm{L}} - \hat\Gamma^{\mathrm{R}})\hat G^<(\varepsilon) + [\hat\Gamma^{\mathrm{L}} f_{\mathrm{L}}(\varepsilon) - \hat\Gamma^{\mathrm{R}} f_{\mathrm{R}}(\varepsilon)][\hat G^{\mathrm{r}}(\varepsilon) - \hat G^{\mathrm{a}}(\varepsilon)]\}. \tag{A.4}$$

To calculate the electric current one should know the lesser, retarded and advanced GFs. Functions G^{r}, G^{a} are determined with use of the equation of motion method, whereas the lesser one is calculated from Keldysh equation $\hat G^< = \hat G^{\mathrm{r}}\hat\Sigma^<\hat G^{\mathrm{a}}$ with the Ng ansatz used for the self-energy $\hat\Sigma^<$ [43].

Functions $G_{ii}(\varepsilon) = \langle\langle d_i, d^\dagger_i\rangle\rangle$ and $G_{-ii}(\varepsilon) = \langle\langle d_{-i}, d^\dagger_i\rangle\rangle$ fulfil the following equations of motion:

$$(\varepsilon - E_i - \Sigma_{0ii})G_{ii} = 1 + UG^{21}_i + (t + \Sigma_{0i-i})G_{-ii} \tag{A.5a}$$

$$(\varepsilon - E_{-i} - \Sigma_{0-i-i})G_{-ii} = UG^{22}_i + (t + \Sigma_{0-ii})G_{ii} \tag{A.5b}$$

with $\Sigma_{0ii'}$ corresponding to the self-energy of the non-interacting system. In the above equations, higher-order GFs appear, namely $G^{21}_i = \langle\langle d_i d^\dagger_{-i} d_{-i}, d^+_i\rangle\rangle$ and $G^{22}_i = \langle\langle d_{-i} d^\dagger_i d_i, d^\dagger_i\rangle\rangle$. The appropriate equation for G^{21}_i takes the form

$$\begin{aligned}(\varepsilon - E_i - U)G^{21}_i = {} & n_{-i} + tG^{22}_i + \sum_{k,\beta}\{T^*_{k\beta i}\langle\langle a_{k\beta} d^\dagger_{-i} d_{-i}, d^\dagger_i\rangle\rangle \\ & - T^*_{k\beta -i}\langle\langle a_{k\beta} d^\dagger_{-i} d_i, d^\dagger_i\rangle\rangle + T_{k\beta -i}\langle\langle a^\dagger_{k\beta} d_i d_{-i}, d^\dagger_i\rangle\rangle\}\end{aligned} \tag{A.6}$$

where $n_i = \langle d^\dagger_i d_i\rangle$ denotes the mean number of electrons in dot i. At relatively high temperatures the Hartree–Fock approach can be introduced to split higher-order functions which contain $a_{k\beta}$, $a^\dagger_{k\beta}$ operators apart from d_i ones. Then, equation (A.6) takes the form

$$(\varepsilon - E_i - U)G^{21}_i = n_{-i}(1 + \Sigma_{0ii}G_{ii} + \Sigma_{0i-i}G_{-ii}) - n_{-ii}(\Sigma_{0-ii}G_{ii} + \Sigma_{0-i-i}G_{-ii}) + tG^{22}_i \tag{A.7}$$

with $n_{-ii} = \langle d^\dagger_{-i} d_i\rangle$. Due to tunnelling processes between dots, the second-order functions G^{21}_i and G^{22}_i are coupled. Writing a similar expression for the function G^{22}_i, one obtains a set of equations which can be easily solved. Finally, the Green function expressed in the matrix form fulfils the following equation of motion (equation (5) in the text)

$$\hat G(\varepsilon) = [\hat I - \hat g(\varepsilon)\hat\Sigma(\varepsilon)]^{-1}\hat g(\varepsilon) \tag{A.8}$$

which corresponds to the Dyson equation with $\hat g(\varepsilon)$ being the GF of the DQD region in the absence of any coupling or interaction and $\hat\Sigma$ represents the appropriate self-energy. Explicit forms of these matrices are given in the text.

References

[1] Johnson A C, Marcus C M, Hanson M P and Gossard A C 2004 *Phys. Rev. Lett.* **93** 106803
[2] Kobayashi K, Aikawa H, Katsumoto S and Iye Y 2002 *Phys. Rev. Lett.* **88** 256806
[3] Zacharia I G, Goldhaber-Gordon D, Granger G, Kastner M A and Khavin Yu B 2001 *Phys. Rev.* B **64** 155311
[4] Gores J, Goldhaber-Gordon D, Heemeyer S, Kastner M A, Shtrikman H, Mahalu D and Meirav U 2000 *Phys. Rev.* B **62** 2188
[5] Kobayashi K, Aikawa H, Katsumoto S and Iye Y 2003 *Phys. Rev.* B **68** 235304
Holleitner A W, Blick R H, Huttel A K, Eberl K and Kotthaus J P 2002 *Science* **297** 70
[6] Holleitner A W, Decker C R, Qin H, Eberl K and Blick R H 2001 *Phys Rev. Lett.* **87** 256802
[7] Loss D and DiVincenzo D P 1998 *Phys. Rev.* A **57** 120
Loss D and Sukhorukov E V 2000 *Phys. Rev. Lett.* **84** 1035
[8] Clerk A A, Waintal X and Brouwer P W 2001 *Phys. Rev. Lett.* **86** 4636
[9] Livermore C, Crouch C H, Westervelt R M, Campman K L and Gossard A C 1996 *Science* **274** 1332
[10] Chen J C, Chang A M and Melloch M R 2004 *Phys. Rev. Lett.* **92** 176801
Jeong H, Chang A M and Melloch M R 2001 *Science* **293** 2221
[11] Rushforth A W, Smith C G, Farrer I, Ritchie D A, Jones G A, Anderson D and Pepper M 2006 *Preprint* cond-mat/0602242
[12] Ramsak A, Mravlje J, Zitko R and Bonca J 2006 *Preprint* cond-mat/0601327
[13] Fransson J and Balatsky A V 2006 *Preprint* cond-mat/0609324
[14] Kubala B and Konig J 2003 *Phys. Rev.* B **65** 245301
Kubala B and Konig J 2003 *Phys. Rev.* B **67** 205303
[15] Ladron de Guevara M L, Claro F and Orellana P A 2003 *Phys. Rev.* B **67** 195335
[16] Kang K and Cho S Y 2004 *J. Phys.: Condens. Matter* **16** 117
[17] Moldoveanu V, Tolea M, Aldea A and Tanatar B 2005 *Phys. Rev.* B **71** 125338
[18] Lu H, Lu R and Zhu B F 2005 *Phys. Rev.* B **71** 235320
[19] Ladron de Guevara M L and Orellana P A 2006 *Phys. Rev.* B **73** 205303
[20] Orellana P A, Ladron de Guevara M L and Claro F 2004 *Phys. Rev.* B **70** 233315
[21] Bai Z-M, Yang M-F and Chen Y-C 2004 *J. Phys.: Condens. Matter* **16** 2053
[22] Dong B, Djuric I, Cui H L and Lei X L 2004 *J. Phys.: Condens. Matter* **16** 4303
[23] Ueda A and Eto M 2006 *Preprint* cond-mat/0601327
[24] Lu H, Lu R and Zhu B F 2006 *Physica* E **34** 538
[25] Trocha P and Barnaś J 2005 *Phys. Status Solidi* c **3** 113
[26] Tanaka Y and Kawakami N 2005 *Phys. Rev.* B **72** 085304
[27] Ding G-H, Kim C K and Nahm K 2005 *Phys. Rev.* B **71** 205313
[28] Stefański P, Tagliacozzo A and Bułka B R 2004 *Phys. Rev. Lett.* **93** 186805
[29] Wu B H and Ahn K-H 2006 *Physica* E **34** 464
[30] Busser C A, Martins G B, Al-Hassanieh K A, Moreo A and Dagotto E 2004 *Phys. Rev.* B **70** 245303
[31] Bułka B R and Stefański P 2001 *Phys. Rev. Lett.* **86** 5128
[32] Torio M E, Hallberg K, Ceccatto A H and Proetto C R 2002 *Phys. Rev.* B **65** 085302
[33] Tanaka Y and Kawakami N 2006 *J. Phys. Soc. Japan* **75** 015004
[34] Hofstetter W, Konig J and Schoeller H 2001 *Phys. Rev. Lett.* **87** 156803
[35] DiVincenzo D P 1995 *Phys. Rev.* A **51** 1015
[36] Lopez R, Sanchez D, Lee M, Choi M S, Simon P and Hur K L 2005 *Phys. Rev.* B **71** 115312
[37] Boese D, Hofstetter W and Schoeller H 2002 *Phys. Rev.* B **66** 125315
[38] Lopez R, Aguado R and Platero G 2002 *Phys. Rev. Lett.* **89** 136802
[39] Meir Y, Wingreen N S and Lee P A 1993 *Phys. Rev. Lett.* **70** 2601
[40] Haug H and Jauho A P 1996 *Kinetics in Transport and Optics of Semiconductors* (Berlin: Springer)
[41] Rudziński W, Barnaś J, Świrkowicz R and Wilczyński M 2005 *Phys. Rev.* B **71** 205307
[42] Sztenkiel D and Swirkowicz R 2007 *Phys. Status Solidi* b at press
[43] Ng T K and Lee P A 1988 *Phys. Rev. Lett.* **61** 1768